Materials Letters 171 (2016) 14–17

Contents lists available at ScienceDirect

Materials Letters

journal homepage: www.elsevier.com/locate/matlet

Carbon uptake and distribution in Spark Plasma Sintering (SPS) processed Sm(Co, Fe, Cu, Zr)$_z$

Alexander J. Mackie [a,*], Gareth D. Hatton [b], Hugh G.C. Hamilton [b], Julian S. Dean [a], Russell Goodall [a]

[a] Materials Science and Engineering, University of Sheffield, Sir Robert Hadfield Building, Mappin Street, S1 3JD Sheffield, UK
[b] Johnson Matthey Technology Centre, Blounts Court Road, Sonning Common, RG4 9NH Reading, UK

ARTICLE INFO

Article history:
Received 13 October 2015
Received in revised form
8 February 2016
Accepted 11 February 2016
Available online 12 February 2016

Keywords:
Spark Plasma Sintering (SPS)
Powder technology
Carbon uptake
Sm(Co, Fe, Cu, Zr)z
Electron probe micro analysis (EPMA)
Magnetic materials

ABSTRACT

Spark Plasma Sintering (SPS) rapidly consolidates high-melting point powders between carbon dies, but carbon can pose a risk for many materials. Carbon uptake in SPS and conventional, pressure-less sintered (CS) Sm(Co, Fe, Cu, Zr)$_z$ has been analysed using Electron Probe Micro-Analysis (EPMA) to produce high-detail elemental distribution maps. Field's metal was used as mounting material to avoid introducing carbon into the samples. The distribution maps show high surface carbon levels in the SPS-processed Sm (Co, Fe, Cu, Zr)z to a depth of 10 μm. Much less carbon was observed in CS Sm(Co, Fe, Cu, Zr)z. Furthermore, elemental carbon analysis (LECO-C) confirmed carbon was most abundant at the surface in SPS-processed Sm(Co, Fe, Cu, Zr)z but also at higher levels internally, when compared to the CS sample. It is inferred that the carbon contamination is due to the contact between the powder and the graphite die/paper at elevated temperatures during SPS process. The measured levels of carbon in the SPS-processed sample are not expected to significantly impact the magnetic properties of Sm(Co, Fe, Cu, Zr)z. These results may have implications for other powder materials processed by SPS with properties sensitive to carbon.

1. Introduction

The SPS technique is a method for processing powders into fully dense compacts much faster than standard conventional processes, such as pressure-less sintering [1,2]. SPS works by applying DC current and uniaxial force to the punch of a powder-containing die and direct heating of the powder allows heating rates of 100 °C and above, which relates to the rapid processing times achieved. This reduced time required for densification at high temperature allows SPS to retain fine microstructures, potentially to the nanoscale [3–5]. These features have garnered SPS a lot of attention as an interesting and attractive alternative to conventional powder processing routes for a number of materials and applications.

Due to the necessity for the die and punches to be electrically conductive and mechanically strong at high temperatures, the material most commonly used is graphite. This choice of material can raise concern, as the powder material is placed in direct contact with carbon at elevated temperatures.

Retained carbon, present after a variety of processing methods, can be detrimental for a number of material properties. For example, the permanent magnet material, Sm(Co, Fe, Cu, Zr)z (commonly used composition of SmCo based magnet) was produced by metal injection molding and shown to retain carbon due to the use of organic binders. In the work of Tian et al. [6], carbon was found to react with the Zr (forming ZrC) and was therefore unavailable to facilitate the formation of the necessary cellular Sm_2Co_{17} and boundary $SmCo_5$ phases in the microstructure during heat-treatment, which are essential for the strong magnetic performance of Sm(Co, Fe, Cu, Zr)z. Increasing the carbon content throughout their composition of Sm(Co, Fe, Cu, Zr)z gradually reduced the hard magnetic properties to zero once carbon within the bulk exceeded 0.49 wt%. Another example of carbon uptake is in SPS-processed spinels and glass-ceramics of a variety of materials, which have reduced transparency due to the carbon contamination. In these studies, the carbon contamination could not be specified to originate from the handling of the powder or due to contact with the high-carbon environment in the SPS process [7–11]. It is therefore crucial to investigate further the extent of carbon uptake during the SPS process to better evaluate the use of SPS as a processing method for high performance magnets and other material applications.

* Corresponding author.
E-mail addresses: Amackie1@Sheffield.ac.uk (A.J. Mackie), gareth.hatton@matthey.com (G.D. Hatton), Hugh.Hamilton@matthey.com (H.G.C. Hamilton), J.dean@Sheffield.ac.uk (J.S. Dean), R.goodall@Sheffield.ac.uk (R. Goodall).

http://dx.doi.org/10.1016/j.matlet.2016.02.049

Two samples of Sm(Co, Fe, Cu, Zr)z, processed via SPS and conventional, pressure-less sintering (CS), have been investigated using Electron Probe Micro-Analysis (EPMA) to acquire precise elemental maps. EPMA can infer the presence of elements as light as carbon [7] and here the distribution of carbon is used to make comparisons between the different processing methods. Samples were mounted in Field's metal (carbon free – polymeric mounting materials contain carbon) to reduce background noise near the sample boundary and remove a potential source of carbon contamination. Quantitative analysis of carbon at the surface, and internally, in both sets of samples was performed using thermal decomposition carbon analysis (LECO-C).

2. Methodology

Standard commercial grade Sm(Co, Fe, Cu, Zr)z-powder was provided by Arnold Magnetic Technologies (Sheffield, UK). For the SPS process, 13 g of Sm(Co, Fe, Cu, Zr)z-Powder was placed inside high-density graphite die (material grade 2333) and lined with 0.35 mm graphite paper, used to facilitate sample removal and protect the die from wear (both provided by Mersen UK). The powder is enclosed by 20 mm diameter graphite punches and subjected to 500 kg (15.6 MPa) cold-press in air (<1 minute) before being transferred to the SPS vessel (FCT Systeme GmbH, Germany). The SPS process occurs in argon atmosphere under the following processing conditions optimized towards full sample density: 100 °C/min heating rate, 1100 °C sintering temperature, 5 min holding time and a maximum pressure of 51 MPa (16 kN). After consolidation, the disc-shaped samples were removed from the die and subjected to a surface polish using 120-grit silicon carbide paper to remove the compacted graphite paper until bare metal was observed, removing on average 0.25mm from each surface. For comparison, Sm(Co, Fe, Cu, Zr)z samples ($18 \times 12 \times 5$mm) produced by pressure-less sintering (powder press, sinter, anneal and finish with a surface polish [12]) were also provided by Arnold Magnetic Technologies.

For EPMA, the two samples were cross-sectioned and mounted within Field's metal (32.5 wt% Bi, 51 wt% In and 16.5 wt% Sn, Alfa Aesar, UK). After surface preparation (finished with 0.4 μm alumina) the samples underwent plasma cleaning to remove remaining polishing remnants. EPMA imaging and elemental mapping was performed using a Jeol JXA-8500 F.

Carbon analysis was performed using LECO CS-844 instrument (AMG-S, Rotherham, England). For this analysis, the SPS-processed and CS Sm(Co, Fe, Cu, Zr)z samples were sectioned and material taken from the middle and at the edges to provide examples of the internal and surface compositions. The internal segments underwent surface polishing to remove 1 mm of material from both the top and bottom faces, to ensure all surfaces were removed. LECO-C relates the amount of carbon present in a sample by thermal decomposition and measurement of the CO_2 levels by infrared absorption [13].

3. Results and discussion

Fig. 1a shows a backscattered SEM image, which contains the Field's metal material (light contrast) and the post surface polish SPS Sm(Co, Fe, Cu, Zr)z (dark contrast). The accompanying carbon map (Fig. 1b) shows a continuous region of carbon distributed along this boundary. Mostly uniform in thickness, the distribution of the carbon extends beyond the defined boundary in Fig. 1a and into the Sm(Co, Fe, Cu, Zr)z region at high levels to an inferred depth of around 10 μm. This observation is consistent in other regions imaged and mapped, although the surface carbon is sometimes less uniform, and can be discontinuous. These findings are consistent with work by Neamţu et al. who obtained EDX distribution maps of carbon in SPS-processed Fe-Si-B glassy powder (consolidated under different SPS processing parameters) and saw carbon detected at the surface of the compacts to a diffusion depth of 2–3 μm [14]. Examples of Inhomogeneity in the Sm(Co, Fe, Cu, Zr)z microstructure (examples highlighted as I, II and III in Fig. 1a), of which EPMA indicates are samarium-rich, correlate with slightly elevated levels of carbon (Fig. 1b) and could potentially be samarium carbide (Sm_3C). If confirmed, the action of carbon in these magnetic materials could be through removal of both samarium and zirconium from the main phase [6]. Also seen in Fig. 1b is a small carbon feature at the top of the Sm(Co, Fe, Cu, Zr)z carbon map, which does not correspond with the backscattered image. It is attributed to be a remnant of dirt/grease. Similar features were not observed in other regions imaged.

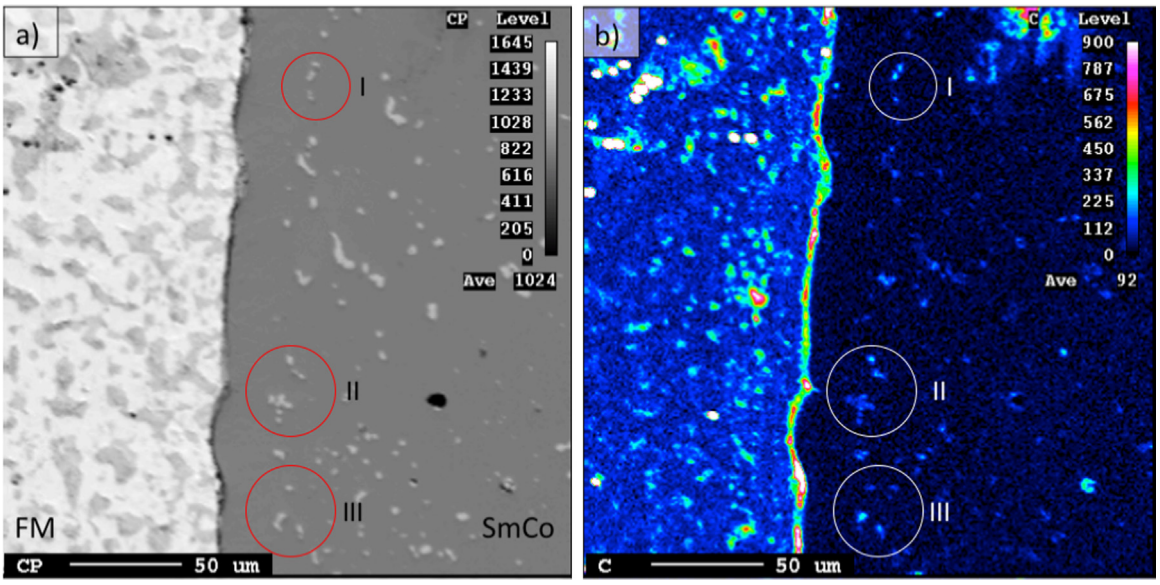

Fig. 1. SEM and EPMA carbon maps for the SPS-processed Sm(Co, Fe, Cu, Zr)z. (a) Backscattered electron mode. Annotations show Field's metal (FM) and Sm(Co, Fe, Cu, Zr)z (SmCo) regions. Imaging is performed after surface polishing. (b) EPMA carbon map of the same region. Carbon uniform and continuous and extends into SmCo region. Inserts (I, II and III) highlight areas rich in Sm (Fig. 1a) coinciding with areas of elevated carbon (Fig. 1b).

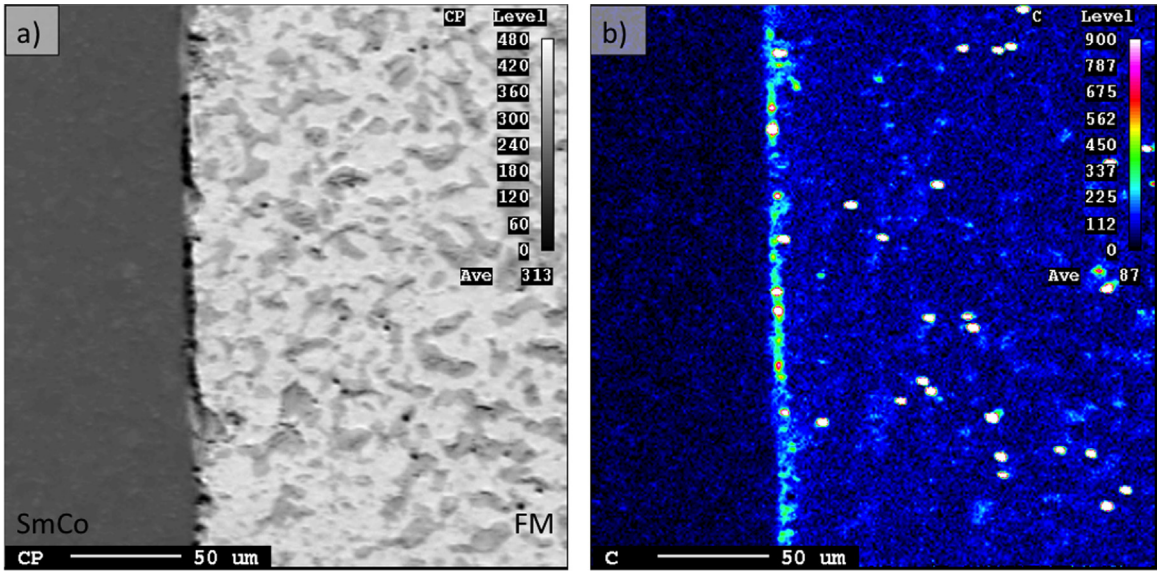

Fig. 2. SEM and EPMA carbon maps for post surface polished conventionally processed Sm(Co, Fe, Cu, Zr)z. (a) Backscattered electron mode. Annotations show Sm(Co, Fe, Cu, Zr)z (SmCo) and Field's metal (FM) regions. (b) EPMA carbon map of the same area. Carbon is discontinuous and confined to the boundary.

Backscattered imaging and EPMA carbon mapping for CS Sm(Co, Fe, Cu, Zr)z sample are shown in Fig. 2. Compared with the SPS-processed sample, carbon is exclusively confined to the Sm(Co, Fe, Cu, Zr)z/Field's metal boundary line and very little, if any, extends into the Sm(Co, Fe, Cu, Zr)z region on the left of Fig. 2b. Beyond the surface, the sample bulk is much more homogenous than the SPS-processed sample and no features of elevated carbon are observed in Fig. 2b. In both samples, carbon is observed within the soft Field's metal; this was obtained at high purity and will be embedded carbon from the surface preparation process.

To compliment the EPMA carbon maps, band profiles (120 μm in width, measuring 1 μm step size from the sample surface into the bulk) were performed (Fig. 3). The SPS sample's band profile shows the distribution of carbon at high levels above background from the sample surface progressing to a depth of 9 μm (HWHM = 7 μm). The small regions of slightly higher carbon content seen in Fig. 1b are not apparent in the band scan. Comparatively, the CS sample band profile displays a slightly elevated peak at the boundary, but within the sample, carbon reduces to background levels much more sharply (HWHM = 3 μm). Compared to the SPS process, pressure-less sintering does not directly encounter a solid carbon material. The source of elevated surface carbon could due to SiC used in the surface polish or from oil-based lubricant used to remove the compact after pressing prior to sintering. The measured background level of carbon is marginally higher in the CS sample, but in both profiles, the background levels are consistent to the maximum examined depth of 160 μm.

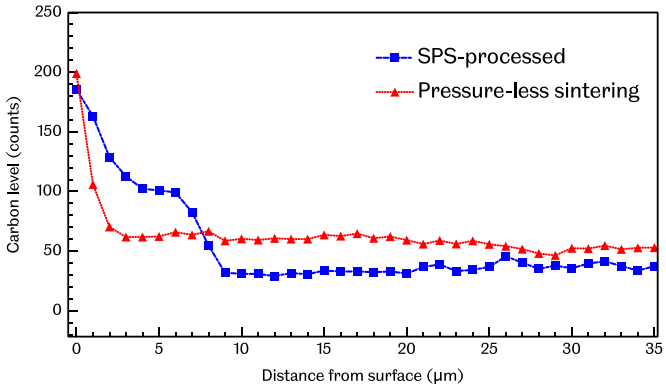

Fig. 3. EPMA band profile data across the Field's metal/Sm(Co, Fe, Cu, Zr)z for both types of processed samples.

Table 1
LECO-C results for internal and surface segments for SPS and conventional sintered Sm(Co, Fe, Cu, Zr)z.

	Internal (wt%) ± 0.006	Surface (wt%) ± 0.006
SPS	0.026	0.035
Conventional sinter	0.016	0.014

Carbon analysis of the internal and surface regions in the SPS and CS samples are shown in Table 1. Measurement of the carbon level in a volume close to the surface of the SPS sample is greater than that measured within the internal region. Similar measurement of carbon in the CS Sm(Co, Fe, Cu, Zr)z shows the weight percentage of elemental carbon measured at the surface and in the central regions to be the same. Carbon is measured higher in both internal and surface regions for the SPS-processed sample, compared to the CS sample, despite the CS background carbon measuring higher in the band scan data. In all cases, the measured weight percentage of elemental carbon in the regions analysed were much smaller when compared to the critical level deemed severely detrimental to the performance of Sm(Co, Fe, Cu, Zr)z of 0.46 wt% [6].

4. Conclusions

Through a variety of analyses, carbon has been shown to contaminate the surface of the Sm(Co, Fe, Cu, Zr)z during the SPS process. For the processing parameters used, EPMA element maps have shown the distribution of highly elevated carbon levels to be limited to visual and measured depths of around 10 μm. Comparison was made with a conventionally processed sample and significantly less carbon was observed beyond the Sm(Co, Fe, Cu, Zr)z/Field's metal boundary. Quantitative analysis via band profiles confirmed these observations. Further quantitative analysis of the carbon at the surface and internally of both samples by LECO-C analysis measured carbon at greater quantities, not only at the surface, but also within the bulk of SPS-processed Sm(Co, Fe, Cu, Zr)z. The levels of carbon measured are not expected to significantly impact the performance of the magnet currently but

further experiments are planned to investigate and confirm this. It was seen from EPMA elemental maps that there is a degree of correlation between high levels of Sm and elevated levels of C beyond the 10 μm surface contamination. Band scans did not detect any significant levels of carbon beyond the 10 μm up to a depth of 160 μm. From this study, we can only confirm the presence of significant carbon can only be confirmed at the surface, indicating the carbon contamination occurs due to contact of the powder with the graphite paper/die wall during the SPS process.

To achieve its hard magnetic properties, Sm(Co, Fe, Cu, Zr)z undergoes a specific heat-treatment (E.g. longest stage: 850 °C for 12 h, before slow cooling to 400 °C and quenched). The surface carbon from the SPS process could potentially move beyond the observed 10 μm penetration depth during the heat-treatment process and hinder the generation of the desired microstructure. Removal of this surface carbon is therefore recommended for SPS processed materials before undergoing further processing. The next stage of this study will focus on the removal of surface carbon and the effect of an extended surface polishing stage on the distribution of the carbon, the phases present and the effect on the magnetic properties of SPS-processed Sm(Co, Fe, Cu, Zr)z.

Acknowledgements

The authors would like to thank Martin Satur and Dr. Urs Wyss of Arnold Magnetic Technologies for providing support during this study. This work is supported by the EU-FP7 Accelerated Metallurgy Project (ACCMET, contract NMP4-LA-2011-263206)ACCMET. One of the authors (AM) would like to acknowledge a studentship provided by THE EPSRC Centre for Doctoral Training in Advanced Metallic Systems (project EP/G036950).

References

[1] J.E. Garay, Current-activated, pressure-assisted densification of materials, Annu. Rev. Mater. Res. 40 (2010) 445–468, http://dx.doi.org/10.1146/annurev-matsci-070909-104433.

[2] R. Orrù, R. Licheri, A.M. Locci, A. Cincotti, G. Cao, Consolidation/synthesis of Materials by electric current activated/assisted sintering, Mater. Sci. Eng. R. Rep. 63 (2009) 127–287, http://dx.doi.org/10.1016/j.mser10.2008.09.003.

[3] N. Lu, X. Song, X. Liu, J. Zhang, Preparation and magnetic properties of amorphous and nanocrystalline Sm(Co, FE, Cu, Zr)z alloys, Intermetallics 18 (2010) 1180–1184, http://dx.doi.org/10.1016/j.intermet.2010.02.034.

[4] S. An, T. Zhang, C. Jiang, Evolution of phase and microstructure in anisotropic nanocrystalline SmCo6.1Si0.9 magnets, J. Appl. Phys. 115 (2014) 043901, http://dx.doi.org/10.1063/1.4862158.

[5] D.T. Zhang, W.C. Lv, M. Yue, J.J. Yang, W.Q. Liu, J.X. Zhang, et al., Nanocrystalline SmCo[sub 5] magnet synthesized by spark plasma sintering, J. Appl. Phys. 107 (2010) 09A701, http://dx.doi.org/10.1063/1.3334458.

[6] J. Tian, S. Zhang, X. Qu, F. Akhtar, S. Tao, Behavior of residual carbon in Sm (Co, Fe, Cu, Zr)z permanent magnets, J. Alloy. Compd. 440 (2007) 89–93, http://dx.doi.org/10.1016/j.jallcom.2006.08.322.

[7] G. Bernard-Granger, N. Benameur, C. Guizard, M. Nygren, Influence of graphite contamination on the optical properties of transparent spinel obtained by spark plasma sintering, Scr. Mater. 60 (2009) 164–167, http://dx.doi.org/10.1016/j.scriptamat.2008.09.027.

[8] A. Bertrand, J. Carreaud, G. Delaizir, J.R. Duclère, M. Colas, J. Cornette, et al., A comprehensive study of the carbon contamination in tellurite glasses and glass–ceramics sintered by spark plasma sintering (SPS), J. Am. Ceram. Soc. 97 (2014) 163–172, http://dx.doi.org/10.1111/jace.12657.

[9] N. Frage, S. Kalabukhov, N. Sverdlov, V. Kasiyan, a. Rothman, M.P. Dariel, effect of the spark plasma sintering (SPS) parameters and LiF doping on the mechanical properties and the transparency of polycrystalline Nd-YAG, Ceram. Int. 38 (2012) 5513–5519, http://dx.doi.org/10.1016/j.ceramint.2012.03.066.

[10] K. Morita, B.-N. Kim, H. Yoshida, K. Hiraga, Y. Sakka, Spectroscopic study of the discoloration of transparent MgAl2O4 spinel fabricated by spark-plasma-sintering (SPS) processing, Acta Mater. 84 (2015) 9–19, http://dx.doi.org/10.1016/j.actamat.2014.10.030.

[11] K. Morita, B. Kim, H. Yoshida, K. Hiraga, Densification behavior of a fine-grained $MgAl_2O_4$ spinel during spark plasma sintering (SPS), SCR. Mater. 63 (2010) 565–568, http://dx.doi.org/10.1016/j.scriptamat.2010.06.012.

[12] S. Constantinides, A Manufacturing and Performance Comparison Between Bonded and Sintered Permanent Magnets, 2006.

[13] M.F. Gazulla, M. Rodrigo, M. Orduña, C.M. Gómez, Determination of carbon, Hydrogen, nitrogen and sulfur in geological materials using elemental analysers, Geostand. Geoanal. Res. 36 (2012) 201–217, http://dx.doi.org/10.1111/j.1751-908X.2011.00140.x.

[14] B.V. Neamţu, T.F. Marinca, I. Chicinaş, O. Isnard, F. Popa, P. Păşcuţă, preparation and soft magnetic properties of spark plasma sintered compacts based on Fe–Si–B glassy powder, J. Alloy. Compd. 600 (2014) 1–7, http://dx.doi.org/10.1016/j.jallcom.2014.02.115.